

# A sulphur abundance study of NGC 300 by an empirical calibration method <sup>\*</sup>

T. Christensen<sup>1,2</sup>, L. Petersen<sup>1</sup>, and P. Gammelgaard<sup>1</sup>

<sup>1</sup> Institut for Fysik og Astronomi, Aarhus Universitet, Ny Munkegade, DK-8000 Århus C, Denmark

<sup>2</sup> Nordic Optical Telescope, Apartado 474, E-38700 Sta. Cruz de La Palma, Spain

Received

; Accepted

**Abstract.** We propose an empirical sulphur abundance determination method based on the strong sulphur emission lines, [S II]  $\lambda\lambda 6716, 6731$  and [S III]  $\lambda\lambda 9069, 9531$  in H II regions. From a compilation of literature data we have made a calibration of sulphur abundance versus  $([\text{S II}] + [\text{S III}])/\text{H}\beta$ , similar to what has been widely used for the more easily observable iso-electronic element oxygen. This enables abundance determinations in extragalactic H II regions without measurements of weak temperature sensitive lines for use in model calculations.

As a first application of the empirical calibration 15 spectra covering the wavelength range 3650–10000 Å have been obtained of H II regions at various galactocentric distances in the spiral galaxy NGC 300, by employing specially designed multiaperture slitmasks which allow simultaneous observations of several H II regions. Sulphur and oxygen abundances are determined and an oxygen gradient in agreement with previously published work is found as well as a somewhat steeper sulphur abundance gradient. This results in a slight decrease of log S/O with increasing radius.

The quite low values of S/O seem to confirm the trend demonstrated by Díaz et al. (1991) of a decrease in log S/O at high metallicities, but still more data are needed before any definite conclusions can be drawn. We find as expected that the radiation softness parameter  $\eta$  decreases with increasing radius and the slope is comparable to what is found for spiral galaxies of similar metallicity.

**Key words:** H II regions – galaxies: abundances – galaxies: NGC 300 – galaxies: spiral

## 1. Introduction

Elemental abundance studies in spiral galaxies have largely been concerned with the abundance of oxygen and the presence of radial O-gradients with negative slopes have been demonstrated for more than a decade. Initiated by the analyses and line ratio calibrations of Edmunds & Pagel (1984) and McCall et al. (1985) large observational samples have recently been compiled by several groups (Vila-Costas & Edmunds 1992; Oey & Kennicutt 1993; Zaritsky et al. 1994, hereafter ZKH), of which the latter collates much of the existing published and their own spectroscopic data on a total of 577 H II regions in 39 spirals.

The present data available through these surveys are of such proportions, that they can address the correlation of oxygen abundance with local and macroscopic parameters of spiral galaxies, which can be used to constrain galaxy evolution models. ZKH define a characteristic oxygen abundance and find that it correlates with galaxy hubble type and luminosity. No clear correlation of oxygen abundance gradients, when expressed as dex/isophotal radius, with Hubble type is seen, although there are indications that intermediate-type spiral galaxies have the steepest gradients and that the slope is flatter in barred than unbarred spirals.

Much less attention has been paid to the sulphur content of spiral galaxies, probably because the strong lines of the ionization stage S<sup>2+</sup> is situated in the near-IR region at  $\lambda = 9069$  and  $9531$  Å, where detector sensibility is low and many atmospheric emission lines are present, although it can give important clues on elemental abundance and the softness parameter as defined in Section 5.1, which was shown by ZKH to increase with decreasing radius, etc.

Garnett (1989) investigates sulphur abundance in 13 extragalactic H II regions and summing up on his own and previous work concludes that there is only very weak if any evidence for gradients in S/O in spiral galaxies. Neither is there a systematic variation of S/O with oxygen abundance even though it might be expected from chemical

---

Send offprint requests to: tina@obs.aau.dk, larsp@obs.aau.dk

<sup>\*</sup> Based on observations obtained with the Danish 1.5-m telescope at ESO, La Silla, Chile

evolution models. In this work we will put more emphasis on the sulphur abundance in spiral galaxies by developing an empirical calibration of sulphur line ratios and abundance.

It has become evident from the studies cited above, that conclusions on abundance variation over a galaxy disk drawn on data from less than five H II regions can be very misleading and even turn out with the wrong sign of the gradient. Therefore more than 10 observed regions per galaxy with good radial coverage is desirable. Ryder (1995), who added oxygen data on 6 new galaxies with findings in support of ZKH, has discussed how H II regions can be observed in a time efficient manner with narrow band filters and multifiber or multislit spectroscopy and pointed out some of the drawbacks of the first two. When broad wavelength coverage of H II regions in nearby galaxies is the objective, multislit spectroscopy might be preferred, since most regions extend over many arcseconds and may be closely situated. Hence, they are not efficiently observed using multifiber spectrographs designed for point-like objects.

NGC 300 is a large, nearby spiral galaxy with many prominent H II regions. At the modest distance of the Sculptor group of galaxies, about 1.2 Mpc, the Scd galaxy extends over 20' and is a perfect object for multislit spectroscopy covering wide fields. By this technique using specially designed multiaperture plates the number of H II regions that can be observed simultaneously is increased as compared to conventional long-slit spectroscopy.

## 2. Line ratios as abundance indicators

Abundances from H II region emission lines are most accurately determined when temperature sensitive lines are measured, since the derived temperature enables modeling of the region. The required lines such as [O III]  $\lambda$ 4363 are, however, quite weak and often not detectable at all. In their absence one has to depend on empirical relationships between the desired abundance and a combination of strong emission lines. Pagel et al. (1979) suggest  $R_{23} = ([\text{O II}] \lambda\lambda 3726, 3729 + [\text{O III}] \lambda\lambda 4959, 5007)/\text{H}\beta$  as an improved oxygen abundance indicator as compared to earlier used line ratios.

A calibration of  $\log(R_{23})$  against oxygen abundance by Edmunds & Pagel (1984) has since been widely used for abundance determinations in regions where the temperature sensitive lines are unreachable. The fit is ambiguous, however, consisting of two branches, and care must be taken to make sure whether the high or low metallicity branch is appropriate in each case. The uncertainty of the abundance is  $\pm 0.2$  dex.

### 2.1. A sulphur abundance indicator

The success of this empirical method of oxygen abundance determination has inspired a similar method for sul-

phur abundance determination. Since these elements are iso-electronic, an expression corresponding to  $R_{23}$  can be made for sulphur, simply by replacing each oxygen line by the corresponding sulphur line. We define:

$$S_{23} \equiv \frac{[\text{S II}] \lambda\lambda 6716, 6731 + [\text{S III}] \lambda\lambda 9069, 9531}{\text{H}\beta}. \quad (1)$$

As two of the sulphur lines are in the far-red part of the spectrum, these have only in the recent years become available, as detector sensibility in this spectral range has been improved. It might be more relevant to normalize  $S_{23}$  to  $\text{H}\alpha$ , the nearest hydrogen Balmer line, than to  $\text{H}\beta$  lying further away in the blue range where it is more sensitive to extinction correction uncertainties. Our spectral resolution, however, is so poor that we can hardly deblend  $\text{H}\alpha$  from the nearby [N II]  $\lambda$ 6548 and [Ne II]  $\lambda$ 6583 lines and thus we find it more reasonable to use  $\text{H}\beta$ . A calibration of  $S_{23}$  versus sulphur abundance should now enable sulphur abundance determinations in H II regions where the weak temperature sensitive line [S III]  $\lambda$ 6312 is undetectable.

A search through literature for the data available for such a calibration has been made. The resulting plot is shown in Fig. 1. All papers have measured values of emission line intensities of the constituent lines of  $S_{23}$  and give from ionization model calculations the sulphur abundance. The data points from Díaz et al. (1991) are from giant H II regions in M51, probably the spiral with the highest abundance known. Their position in the plot suggests that they belong to a high metallicity branch, whereas all other data points seem to fit nicely on a low metallicity branch. It seems likely that only extremely high metallicity H II regions will be on the high metallicity branch. The majority of H II regions will fit on the lower branch and thus only for this branch a fit is made. A first order weighted fit gives:

$$\log(\text{S}/\text{H}) + 12 = 6.485 + 1.218 \log(S_{23}). \quad (2)$$

In addition a grid of model H II regions from Stasinska (1990) has been plotted in the diagram. All models have one ionizing star and both models with uniform hydrogen number density 10 and 1000  $\text{cm}^{-3}$  have been included. The horizontal dispersion is mainly due to the effective temperature of the ionizing star varying from 32500 to 55000 K. The theoretical models further consolidate the lower branch and suggest the existence of a higher branch. The latter, however, has as yet a quite diffuse appearance.

All papers used for this plot except Pastoriza et al. (1993) have taken into account the possible contribution of  $\text{S}^{3+}$  to the sulphur abundance. All but one of their regions have so large  $\text{O}^+/\text{O}$  ratios ( $> 0.5$ ) that  $\text{S}^{3+}$  is not likely to be present in significant amounts (Garnett 1989). The rightmost of the datapoints in Fig. 1 has considerably

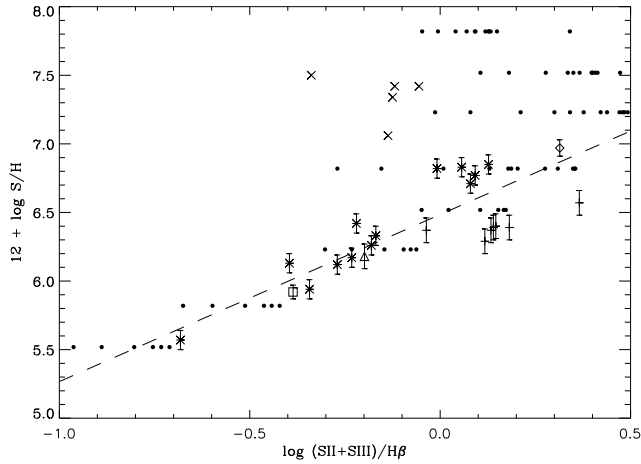


**Fig. 1.** Sulphur abundance as a function of  $S_{23}$ .  $\times$ : Díaz et al. (1991).  $*$ : Garnett (1989).  $\Delta$ : Garnett & Kennicutt (1994).  $\diamond$ : Osterbrock et al. (1992).  $+$ : Pastoriza et al. (1993).  $\square$ : Skillman et al. (1994).  $\bullet$ : Theoretical models from Stasinska (1990), not included in the fit. The dashed line is the fit given in Eq. (2).

higher ionization (as it is a region in the nucleus), and  $S^+ + S^{2+}$  might not contribute more than 80 % of the total sulphur abundance.

### 3. Observations

The observations were carried out at the Danish 1.5-m telescope at ESO, La Silla, Chile, where a facility to exploit multislit spectroscopy with the Danish Faint Object Spectrograph and Camera (DFOSC) is under development. The CCD available at the time of observation (Thompson  $1k \times 1k$ ) had a field size of  $8'.6 \times 8'.6$ , large enough to include the main parts of the galaxy. The aperture plates are manufactured on site from a hard plastic material with a milling machine controlled by an instruction file generated on the basis of well-sampled  $H\alpha$ -exposures obtained with the same instrument.

NGC 300 was observed during 2 nights in July 1995 (see Table 1). Two different aperture plates were used, both having 8 non-overlapping slitlets with widths of  $\simeq 2''.5$ . The number and lengths of the slitlets were governed by the wish to maximize the number of H II regions observed in one exposure and the need to have sufficiently sampling of the galaxy stellar continuum and the local sky background, which is especially important in the near-IR range where emission from atmospheric OH-lines rises strongly. Since some regions have large angular sizes and some slitlets included two regions these criteria were met using lengths of  $30\text{--}60''$ . One slitlet was positioned to contain pure sky background for comparison, but the use of such a global sky spectrum gave generally a poorer background subtraction, presumably due the low spectral

resolution (see below) and the displacement of the spectra in the dispersion direction.

In total spectra of 14 H II regions were obtained with the two aperture plates; region 137A appears in the observations from both nights due to an initial misidentification. With exposure times of 3000–7000 s the advantage of simultaneous observation of 5–10 H II regions compared to long-slit spectroscopy is obvious. Unfortunately the achieved spectral resolution was rather low,  $\sim 25 \text{ \AA}$  and  $\sim 60 \text{ \AA}$  in the blue and red ranges respectively, due to a malfunction of the best suited grisms. This means that  $[S II] \lambda\lambda 6716, 6731$  must be deblended from the He I line at  $6678 \text{ \AA}$  and the flux of weak Paschen lines must be subtracted from the  $[S III]$  lines.

### 4. Data reductions

The multiaperture CCD frames were reduced by employing standard IRAF packages for flat-fielding, extraction of one-dimensional spectra, calibration etc. Since the slitlets cannot be milled with exactly the same widths special care must be taken in the reduction process. Pixel-to-pixel variations are removed by normalizing the spectrum from each slitlet using well-exposed dome flat-fields made through the same instrumental setup. Long range variations over the CCD are accounted for by normalizing the collapsed one-dimensional spectra from each slitlet of a twilight sky exposure with the signal of the slitlet through which the flux standard star exposures are taken. This last procedure is similar to the illumination correction applied in long-slit spectroscopy.

The wavelength calibration was performed on the extracted one-dimensional spectra using He lamp exposures, both for the blue and red wavelength range, obtained through the slitlet mask right after the science frames, while the telescope was pointing in the same direction to minimize any effect of flexure. Multiple exposures of the spectrophotometric standard star LTT 377 (Stone & Baldwin 1983, Baldwin & Stone 1984) from each night were used to convert to absolute flux. The effect of atmospheric refraction (Fillipenko 1982) was negligible with the employed slit width, since both NGC 300 and LTT 377 were observed at low airmasses ranging between 1.03–1.08. The blue and red spectra overlap in the region  $5300\text{--}6200 \text{ \AA}$ , which can be used to test the reliability of the flux calibration. Generally the deviation between the two ranges is less than 5 % (see Figure 2) and the mean difference for the apertures with high S/N is  $\leq 2\%$  for both nights, so no correction factor are applied when the two parts of the spectrum are merged.

In the near-IR spectral range careful measures were taken to remove the effect of the atmospheric  $H_2O$  absorption band at  $\lambda\lambda 8900\text{--}9800$  using the procedure proposed by Osterbrock et al. (1990). After fitting a smooth global continuum the line fluxes were measured by fitting a Gaussian profile to the line, or two Gaussians if deblend-

**Table 1.** Log of observations

Date	H II regionID <sup>a</sup>	Wavelengths (Å)	exp. time (s)
July 30 1995	45,61,77,79,109,118A,127,137A	3650–6200	2700
July 30 1995	do.	5300–10000	4500
July 31 1995	53AB,76A,88+90,100,119A,137A,137C	3650–6200	4800
July 31 1995	do.	5300–10000	7200

<sup>a</sup> Identification of the individual H II regions follows the numbering by Deharveng et al. (1988)

ing from nearby lines is relevant, and integrating under these profiles.

Finally the measured line fluxes are corrected for interstellar extinction by determination of the visual extinction,  $A_V$ , using the line flux of  $H\delta$ ,  $H\gamma$ ,  $H\beta$  and  $H\alpha$ , and where possible the Paschen line P9, with the method described by Petersen & Gammelgaard (1996) assuming  $T_e = 10^4$  K and  $n_e = 10^2$  cm<sup>-3</sup> for the giant H II regions. For those H II regions where the extinction determination does not seem to be reliable, values of  $A_V$  have been adopted from D’Odorico et al. (1983) and Webster & Smith (1983) if available, or as a simple average of the other regions.

The data reduction can be tested by comparing the ratio of the two near-IR [S III] lines with the theoretical ratio of 2.48 (Mendoza & Zeppen 1982). We find a mean value for  $I(\lambda 9531)/I(\lambda 9069)$  of  $2.78 \pm 0.15$ , i.e. 12 % above the theoretical ratio. In fact this deviation is quite small giving us faith that our correction for the atmospheric H<sub>2</sub>O absorption band and blending by OH emission lines has been successful in spite of the low spectral resolution we were forced to use. This is probably due to the fact that both [S III]  $\lambda$  9069 and [S III]  $\lambda$  9531 are fortuitously positioned at wavelengths where atmospheric effects are relatively low as evident from the plots in Osterbrock et al. (1990) and Osterbrock & Martel (1992). We are therefore confident that the sulphur line fluxes can be assessed with sufficient accuracy for the present study.

## 5. Results

An example of the final reduced spectra is shown in Fig. 2. In the region 5300–6200 Å, covered by both the blue and the red exposure, the success of the flux calibration is demonstrated by the closely coinciding spectral parts. In Table 2 the extinction and water absorption corrected line intensities relative to  $H\beta$  are listed along with the absolute  $H\beta$ -flux and the extinction in V. The underlying Paschen hydrogen emission has been subtracted from the [S III] line fluxes by means of the theoretical line ratios from Hummer & Storey (1987), assuming physical properties as mentioned above for the extinction determination.

An exact uncertainty calculation for the line intensities is very hard to carry out due to the many sources

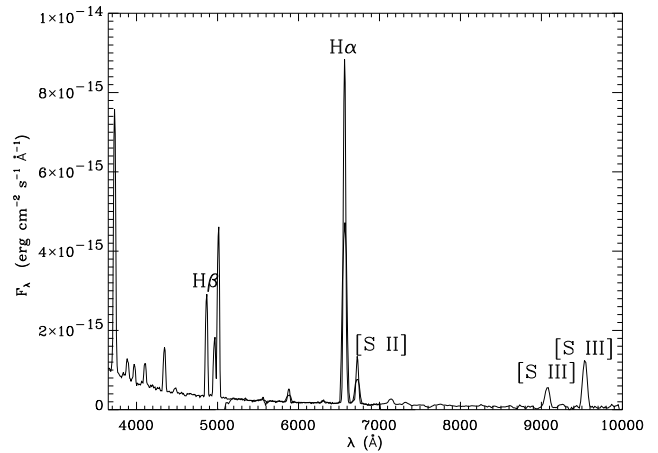


**Fig. 2.** Combined spectrum of the region 53A, B. Notice how smoothly the blue and red part of the spectrum merge. In the overlapping region the difference in resolution is obvious. The most important lines are labeled.

of uncertainty in the reduction steps and the deblending procedure. Consequently we have assigned uncertainties to the lines following these qualitative guidelines inspired by Ryder (1995): when S/N is high and the lines easily identified we assess a relative uncertainty of 15 % and when the lines could only just be distinguished from the noise we adopt a relative uncertainty of 30 %. In the case of  $H\alpha$  the uncertainty assigned is 30 % due to problematic deblending from nearby lines.

The agreement between the observations from the two nights might be tested by comparing the two measurements of region 137A. The spectrum from July 31st (listed first in Table 2) has somewhat higher resolution and the value of  $A_V$  derived from these data has been used for both spectra. The relative line intensities for [O II] and [S II] are lower the second night while the lines from the double-ionized stages are considerably higher (20 % for [O III] and 35 % for [S III]). This is more than the expected uncertainty and suggests that the two slitlet positions do not coincide as we see a higher ionization the second night and furthermore a much lower absolute  $H\beta$ -intensity.

**Table 2.** Corrected line intensities

Region:	45	53A, B	61	76A	77	79	88, 90	100
[O II] $\lambda\lambda 3726, 3729$	3.441	3.507	2.553	3.103	2.365	3.018	4.366	2.034 <sup>a</sup>
H $\delta$	0.293 <sup>a</sup>	0.294					0.419	
H $\gamma$	0.477	0.494		0.055 <sup>a</sup>				
H $\beta$	1.000	1.000	1.000	1.000	1.000	1.000	1.000	1.000 <sup>a</sup>
[O III] $\lambda 4959$	0.105 <sup>a</sup>	0.549	0.481	0.123 <sup>a</sup>	0.464	0.380	0.254	0.221 <sup>a</sup>
[O III] $\lambda 5007$	0.368 <sup>a</sup>	1.580	1.503	0.297 <sup>a</sup>	1.421	1.105	0.696	0.789 <sup>a</sup>
H $\alpha$	1.81 <sup>a</sup>	2.25 <sup>a</sup>		2.28 <sup>a</sup>			2.18 <sup>a</sup>	
[S II] $\lambda\lambda 6716, 6731$	0.623	0.344	0.292	0.478	0.376	0.458	0.578	0.821 <sup>a</sup>
[S III] $\lambda 9069$	0.168 <sup>a</sup>	0.217	0.214	0.285	0.164	0.175	0.169	0.557 <sup>a</sup>
P9	0.042 <sup>a</sup>	0.038		0.038 <sup>a</sup>				
[S III] $\lambda 9531$	0.331	0.484	0.516	0.860	0.348	0.370	0.527	1.807 <sup>a</sup>
$-\log I(\text{H}\beta)$	13.07	13.96	13.62	14.51	13.19	13.28	13.96	13.43
$A_V$	1.04	0.91	0.87 <sup>d</sup>	0.89	0.86 <sup>b</sup>	1.01 <sup>b</sup>	1.23	0.79 <sup>c</sup>

Region:	109	118A	119A	127	137A	137A	137C
[O II] $\lambda\lambda 3726, 3729$	3.293	2.205	3.151	1.955	1.750	2.094	2.523
H $\delta$		0.226	0.254 <sup>a</sup>		0.321 <sup>a</sup>		
H $\gamma$		0.497	0.435		0.429		0.497 <sup>a</sup>
H $\beta$	1.000	1.000	1.000	1.000	1.000	1.000	1.000
[O III] $\lambda 4959$	0.163 <sup>a</sup>	0.597	0.348	0.747	0.862	0.724	0.625
[O III] $\lambda 5007$	0.588 <sup>a</sup>	1.771	1.041	2.293	2.583	2.125	2.030
H $\alpha$			2.80 <sup>a</sup>		2.18 <sup>a</sup>		2.31 <sup>a</sup>
[S II] $\lambda\lambda 6716, 6731$	0.582	0.291	0.467	0.302	0.162	0.172	0.224
[S III] $\lambda 9069$	0.101 <sup>a</sup>	0.175	0.223	0.220 <sup>a</sup>	0.270	0.198	0.114 <sup>a</sup>
P9		0.028 <sup>a</sup>	0.024 <sup>a</sup>		0.027 <sup>a</sup>		0.032 <sup>a</sup>
[S III] $\lambda 9531$	0.303	0.586	0.845	0.462	0.775	0.578	0.406
$-\log I(\text{H}\beta)$	13.42	13.17	13.74	13.70	13.14	13.79	13.18
$A_V$	1.22 <sup>b</sup>	0.79	0.42	0.87 <sup>d</sup>	0.67	0.67	1.70

<sup>a</sup> Uncertainty estimated to 30 %. Elsewhere 15 %.<sup>b</sup> From D'Odorico et al. (1983).<sup>c</sup> From Webster and Smith (1983).<sup>d</sup> Average of the other regions.

From the line intensities the parameter  $S_{23}$  is calculated according to Eq. (1) and plotted versus radial distance from the center of the galaxy in Fig. 3. The deprojected fractional isophotal radii  $\rho/\rho_o$ , where the isophotal radius is the distance where the surface brightness equals 25 mag/arcsec<sup>2</sup>, are taken from Deharveng et al. (1988). For NGC 300  $\rho_o = 9'.75$ . This normalization radius is less sensitive to selection effects, when comparing physical properties of spiral galaxies. The uncertainty calculation for  $S_{23}$  takes into account the uncertainty of the extinction and the estimated uncertainty of the line fluxes. From Fig. 3 a gradient in  $S_{23}$  is evident. A linear weighted fit gives  $\log S_{23} = 0.40 \pm 0.09 - (1.03 \pm 0.29)\rho/\rho_o$ . By means of the relation in Eq. (2) this is converted to a sulphur abundance gradient:

$$12 + \log \left( \frac{S}{H} \right) = 6.97 \pm 0.14 - (1.25 \pm 0.38) \rho/\rho_o \quad (3)$$

For the rather high  $S_{23}$ -values we find, one might wonder whether the regions could belong to the (as yet indefinite) high metallicity branch in Fig. 1 in stead of the lower branch where our Eq. (2) is valid. However, since we find a decrease in  $S_{23}$  with radius, only the lower branch is consistent with a decreasing sulphur abundance gradient which ensures us that our assumption is correct. A fit to the high branch would be inversely proportional to the abundance and would result in a sulphur abundance gradient increasing with radius in contradiction with all expectations.

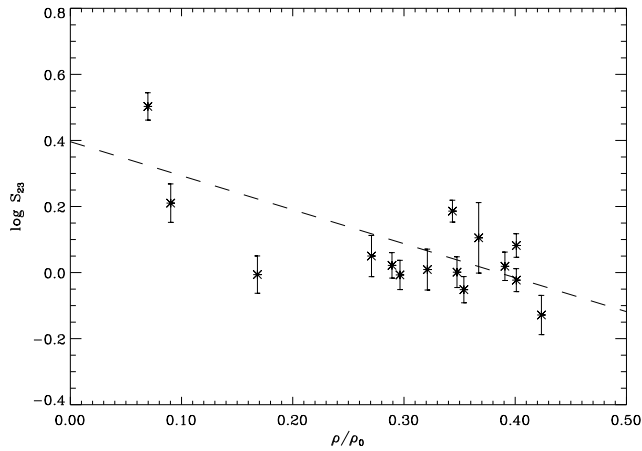
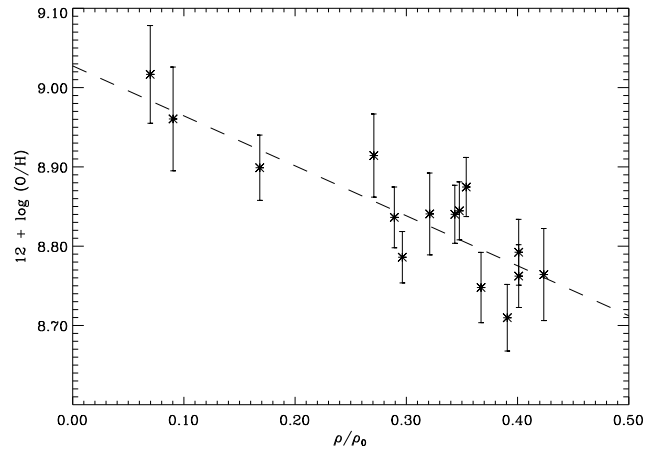
From the observed oxygen line fluxes the parameter  $R_{23}$  is calculated. The calibration by ZKH of  $R_{23}$  versus

**Table 3.** Abundances

Region:	45	53A, B	61	76A	77	79	88, 90	100
$\rho/\rho_o^a$	0.27	0.39	0.32	0.09	0.35	0.35	0.37	0.07
$12 + \log O/H^b$	8.91	8.71	8.84	8.96	8.87	8.84	8.75	9.02
$12 + \log S/H^c$	6.55	6.51	6.50	6.74	6.42	6.49	6.61	7.10
$-\log S/O^c$	2.37	2.20	2.34	2.22	2.45	2.36	2.13	1.92

Region:	109	118A	119A	127	137A	137A	137C
$\rho/\rho_o^a$	0.17	0.29	0.34	0.30	0.40	0.40	0.42
$12 + \log O/H^b$	8.90	8.84	8.84	8.79	8.76	8.79	8.76
$12 + \log S/H^c$	6.48	6.51	6.71	6.48	6.58	6.46	6.33
$-\log S/O^c$	2.42	2.32	2.13	2.31	2.18	2.34	2.44

<sup>a</sup> From Deharveng et al. (1988).<sup>b</sup> Uncertainty estimated to  $\pm 0.2$  dex.<sup>c</sup> Typical uncertainty:  $\pm 0.3$  dex.**Fig. 3.** The variation of the parameter  $S_{23} = ([S II] + [S III])/H\beta$  across NGC 300. The abscissa gives the radial distance  $\rho$  in units of the isophotal radius  $\rho_o$ . The dashed line is the best linear fit given in Eq. (3).**Fig. 4.** The oxygen abundance gradient in NGC 300. The abscissa gives the radial distance  $\rho$  in units of the isophotal radius  $\rho_o$ . The dashed line is the best linear fit given in Table 4.

oxygen abundance is employed and the resulting plot of oxygen abundance versus radius shows a clear trend of decreasing abundance with growing radius (Fig. 4). In Table 3 the calculated abundances for each region are given as well as the isophotal radii. The calculated abundance gradients are given in Table 4 together with results for oxygen from previous work. There is a fine agreement between the results.

Comparing the gradients in Figs. 3 and 4 it is seen that the oxygen abundance gradient is more well-determined than the one for sulphur. This is most likely due to the much lower resolution of the red spectrum where all the sulphur lines are located as compared to the blue spectrum where all the oxygen lines lie.

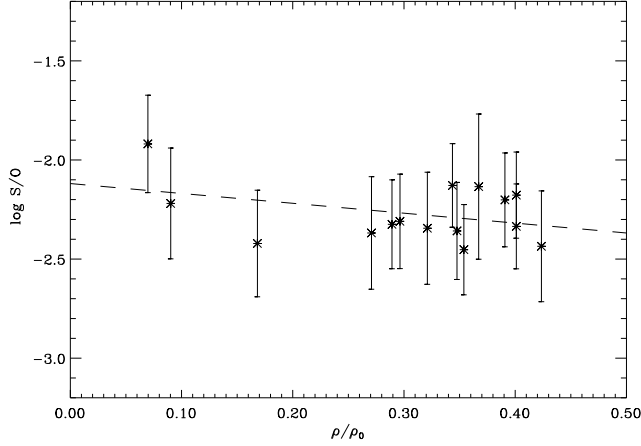
As the sulphur abundance has a steeper slope than the oxygen abundance we find a slight decrease in  $S/O$  as the radius increases as can be seen in Fig. 5. The value of the gradient is given in Table 4.

From Fig. 3 it is apparent that the value of the sulphur abundance gradient is quite dependent on the innermost datapoint. If this region (# 100) is omitted the gradient is drastically reduced to  $-0.43 \pm 0.37$  dex/ $\rho_o$ , indicating that the uncertainty of the gradient might very well be greater than that quoted in Table 4. We do not, however, especially mistrust our observations of this region. Even though it has the weakest emission of our sample the S/N of the spectrum is acceptable. To firmly establish the value of this gradient observations of more regions at large radial

**Table 4.** Abundance gradients in NGC 300

Source	Abundance gradient
This work	$12 + \log (S/H) = (6.97 \pm 0.14) - (1.25 \pm 0.38) \rho/\rho_o$
This work	$12 + \log (O/H) = (9.03 \pm 0.04) - (0.63 \pm 0.13) \rho/\rho_o$
This work	$\log S/O = (-2.12 \pm 0.11) - (0.50 \pm 0.35) \rho/\rho_o$
Deharveng et al. (1988)	$12 + \log (O/H) = (8.95 \pm 0.04) - (0.63 \pm 0.10) \rho/\rho_o$
Zaritsky et al. (1994) <sup>a</sup>	$12 + \log (O/H) = (8.97 \pm 0.04) - (0.61 \pm 0.05) \rho/\rho_o$

<sup>a</sup> Based on the combined data from Webster and Smith (1983), Pagel et al. (1979) and Deharveng et al. (1988).

**Fig. 5.**  $\log S/O$  plotted vs. fractional isophotal radius  $\rho/\rho_o$ . The dashed line represents the best linear fit, see Table 4.

distances as well as at small distances are needed (preferably at a higher resolution).

The same sensitivity to this innermost datapoint is displayed by the gradient in Fig. 5. When the S/O gradient is calculated with region 100 omitted the result is  $+0.12 \pm 0.36$  dex/ $\rho_o$ , i.e. a radial gradient in S/O is no longer present.

If a relation between  $\log S/O$  and oxygen abundance could be established a powerful tool to test galactic chemical evolution models would be at hand. Sulphur is produced in stars with  $M > 10 M_\odot$  and the ratio of sulphur to oxygen produced is greatest in stars with masses in the range 12–20 solar masses. Variations in  $\log S/O$  vs. metallicity could thus reflect variations in the IMF. Garnett (1989). Investigations of this relationship has been made by Garnett (1989) and Díaz et al. (1991). The former find no evidence for a relation while the latter investigates more metal rich regions and find a decrease at high metallicities. Our data confirm the trend demonstrated by Díaz et al. (1991) of a decrease in  $\log S/O$  at high oxygen abundance. We do, however, find quite low S/O-values in comparison with their collection of data, but keeping the rather large uncertainties (including both uncertainties of

the fluxes and the fit in Eq. (2)) in mind, the discrepancy might not be significant.

### 5.1. The softness and ionization parameters

Some of the physical parameters determining the H II region spectra are the ionization parameter  $u$  and the ionizing spectrum characterized by the mean effective temperature  $T_\star$  of the ionizing stars. Vílchez & Pagel (1988, hereafter VP) introduced the parameter  $\eta = (O^+/O^{2+})/(S^{2+}/S^+)$ , which was shown to have a one-to-one relation with  $T_\star$ , as an indicator of the radiation softness. It has the important advantages of being insensitive to density and virtually independent of  $u$  and  $T_e$ . The actual relationship with  $T_\star$  depend on stellar model atmosphere calculation.

As discussed by Garnett (1989) it is still premature to make any quantitative assessment of  $T_\star$  from  $\eta$  and more detailed non-LTE models of hot stars are required to derive absolute values of the effective temperature of the ionizing sources. Nevertheless, he argues that  $\eta$  can still be used as a sequencing parameter to examine the relative behaviour of  $T_\star$ , and we shall use it to investigate the gross properties of  $T_\star$  in NGC 300. When the near-IR [S III] lines are available  $\eta$  is easily found from the observable line ratio quotient (VP):

$$\eta' = \frac{[O II] \lambda\lambda 3726, 3729}{[O III] \lambda\lambda 4959, 5007} \bigg/ \frac{[S II] \lambda\lambda 6717, 6731}{[S III] \lambda\lambda 9069, 9531} \quad (4)$$

through the relation

$$\log \eta = \eta' + 0.14/t + 0.16, \quad (5)$$

where  $t = T_e/10^4 K$ . We used the value  $t = 1.0$  for all H II regions rather than acquiring  $T_e$  from various sources, since any variation of  $t$  in the range 0.7–1.4 will only result in a change in  $\log \eta$  of 0.1 dex (VP), less than the observational errors, and the few regions that have  $T_e$  determined in the literature (Webster & Smith 1983; Pagel et al. 1979) are all in the range 8000–11000 K.

In Fig. 6 we plot the deduced  $\eta$ -parameter for the H II regions in NGC 300 versus fractional isophotal radius which can be compared to Fig. 5 of ZKH. Our data

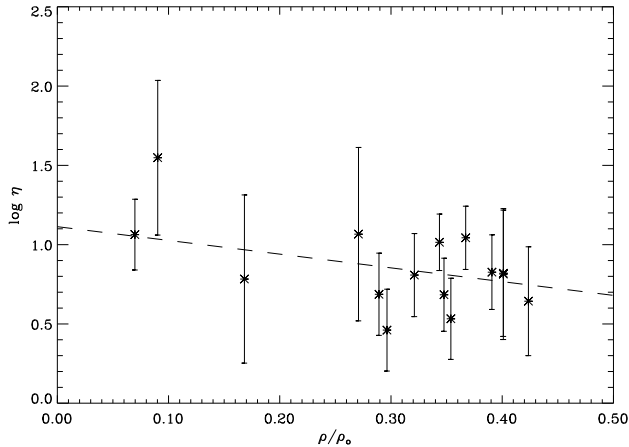


**Fig. 6.** The softness parameter  $\eta$  plotted vs. the fractional isophotal radius  $\rho/\rho_o$ . The dashed line represents the best linear fit.

points fall in the bulk of their measurements for seven spiral galaxies between  $\rho/\rho_o = 0-0.5$ , thus falling below the original fit to M33 and M101 by VP. Given the uncertainties in all works discussed here this might not be significant, though. We confirm for NGC 300 the general trend of decreasing  $\log \eta$  with increasing radius.

VP interpret a correlation of  $\log \eta$  with oxygen abundance in the sense that at low oxygen abundance stars tend to be hotter, as a result of an IMF depending on abundance, possibly with some scatter related to evolution. This implies that for galaxies with steep abundance gradient one expect to find gradients in  $T_*$  and likewise in  $\eta$ , while low-abundance galaxies with no distinctive gradient only will show a scatter due to mixing of evolutionary stages. When compared to the plot by ZKH NGC 300 indeed seems to have an intermediate slope of the  $\log \eta$ -gradient resembling maybe that of NGC 2903 and NGC 4559, which have similar oxygen gradients and shallower than the fit for M33 and M101, which also have the steepest oxygen gradients.

The ionization parameter may be calculated from the ratio of the [S II] and [S III] lines through the relationship given by Díaz et al. (1991)

$$\log u = -1.68 \log \left( \frac{[\text{S II}] \lambda\lambda 6717, 6731}{[\text{S III}] \lambda\lambda 9069, 9531} \right) - 2.99, \quad (6)$$

valid for  $\log([\text{S II}]/[\text{S III}]) \simeq -0.5 - 1.0$ . The values of  $\log u$  fall in the range  $-1.6$  to  $-3.3$  with most of the regions scattered around  $-2.5$ , thus justifying the use of Eq. (6). No trend with isophotal radius was seen as was also the case for the seven spiral galaxies where  $u$  has been investigated by ZKH.

## 6. Conclusion

The observations of NGC 300 have demonstrated the advantage of the MOS facility for spectroscopy of extragalactic H II regions, where 15–20 regions distributed over a wide field can be included in only two exposures. In this setup the individual slitlets can be made sufficiently long to enable a good sampling of the local sky background, which is necessary to obtain precise spectra at all wavelengths in the range 3650–10000 Å.

We have successfully applied a new sulphur abundance determination scheme based on the strong [S II] and [S III] emission lines to H II regions in the spiral galaxy NGC 300 in spite of the very poor resolution attainable at the time of the observations. The regions exhibit a clear trend of decreasing sulphur abundance with increasing galactocentric distance with a gradient of  $-1.25 \pm 0.38 \text{ dex}/\rho_o$ , as well as a distinct oxygen abundance gradient. It is assuring that the latter is consistent with previous work (Table 4). Quite low S/O-values for NGC 300 are derived in support of the decrease found by Díaz et al. (1991) at high metallicity but any certain conclusions on this issue must await more data from a larger sample of galaxies. The radiation softness parameter seems to have a gradient with a slope equal to galaxies of similar oxygen abundance gradients.

The sulphur abundance gradient found in this project could be improved by including regions with  $\rho/\rho_o > 0.5$ , preferably at distances at or beyond  $\rho_o$ . With the large field size and sensitivity of the CCD's now used, multi-slit spectroscopy will undoubtedly be a powerful tool for abundance studies in spiral galaxies.

In the future we will apply our empirical sulphur abundance method to H II regions in other spirals. Hopefully further detailed studies of sulphur abundance in bright H II regions will lead to an improvement of the calibration of the suggested empirical sulphur abundance indicator,  $S_{23}$ .

*Acknowledgements.* We highly appreciate the advices concerning the MOS facility at the Danish 1.5-m telescope at ESO, La Silla by Michael I. Andersen, without whom the multislit observations could not have been accomplished. This project was supported by the Danish Board for Astronomical Research.

## References

- Baldwin J.A., Stone R.P.S. 1984, MNRAS 206, 241
- Deharveng L., Caplan J., Lequeux J., et al. 1988, A&AS 73, 407
- Díaz A.I., Terlevich E., Vílchez J.M., Pagel B.E.J., Edmunds M.G. 1991, MNRAS 253, 245
- D'Odorico S., Rosa M., Wampler E.J. 1983, A&AS 53, 97
- Edmunds M.G., Pagel B.E.J. 1984, MNRAS 211, 507
- Fillipenko A.V. 1982, PASP 94, 715
- Garnett D.R. 1989, ApJ 345, 282
- Garnett D.R., Kennicutt Jr. R.C. 1994, ApJ 426, 123
- Hummer D.G., Storey P.J. 1987, MNRAS 224, 801
- McCall M.L., Rybski P.M., Shields G.A. 1985, ApJS 57, 1



- Mendoza C., Zeippen C.J. 1982, MNRAS 198, 127
- Oey M.S., Kennicutt Jr. R.C. 1993, ApJ 411, 137
- Osterbrock D.E., Martel A. 1992, PASP 104, 76
- Osterbrock D.E., Shaw R.A., Veilleux S. 1990, ApJ 352, 561
- Osterbrock D.E., Tran H.D., Veilleux S. 1992, ApJ 389, 305
- Pagel B.E.J., Edmunds M.G., Blackwell D.E., Chun M.S., Smith G. 1979, MNRAS 189, 95
- Pastoriza M.G., Dottori H.A., Terlevich E., Terlevich R., Díaz A.I. 1993, MNRAS 260, 177
- Petersen L., Gammelgaard P. 1996, A&A 308, 49
- Ryder S.D. 1995, ApJ 444, 610
- Skillman E.D., Terlevich R.J., Kennicutt Jr. R.C., Garnett D.R., Terlevich E. 1994, ApJ 431, 172
- Stasinska G. 1990, A&AS 83, 501
- Stone R.P.S., Baldwin J.A. 1983, MNRAS 204, 347
- Vila-Costas M.B., Edmunds M.G. 1992, MNRAS 259, 121
- Vílchez J.M., Pagel B.E.J. 1988, MNRAS 231, 257 (VP)
- Webster B.L., Smith M.G. 1983, MNRAS 204, 743
- Zaritsky D., Kennicutt Jr. R.C., Huchra J.P. 1994, ApJ 420, 87 (ZKH)